APPENDIX V
Publication P5

Burakov, A., Arkkio, A. 2007. Low-order parametric force model for eccentric-rotor electrical machine equipped with parallel stator windings and rotor cage. *IET Electric Power Applications*, Vol. 1, Issue 4, pp. 532-542.

Low-order parametric force model for eccentric-rotor electrical machine equipped with parallel stator windings and rotor cage

A. Burakov and A. Arkkio

Abstract: In the paper, a new low-order parametric force model for an electrical machine with eccentric rotor is developed and verified. The model is designed for an electrical machine equipped with both the parallel stator windings and rotor cage, and, therefore, accounts for the equalising currents in the stator and rotor windings separately and also for their influence on each other. Furthermore, the model can also be used with an electrical machine having either the parallel stator windings or the rotor cage. The presented model with parameters estimated from the numerical test results demonstrated a very good performance in a wide whirling frequency range. The proposed model provides an opportunity to combine effectively the electromagnetic and mechanical analyses of the electrical machine.

1 Introduction

An eccentric rotor motion (also called 'rotor whirling') occurs when the rotor axis of an electrical machine does not coincide with the axis of the stator bore, but, instead, travels around the latter at a certain radius and angular speed (called 'whirling radius' and 'whirling angular speed', respectively). Owing to manufacturing tolerances, wear of bearings and other reasons, some degree of rotor eccentricity is always present. Rotor eccentricity generates the electromagnetic force (also known as unbalanced magnetic pull, UMP) that acts between the rotor and stator. The amplitude and direction of this force depend on the operating characteristics of the motor, whirling frequency and radius. Acting roughly in the direction of the shortest air gap, the UMP tries to further increase the eccentricity magnitude and may cause serious damage to the machine or even the whole drive.

The occurrence and effects of an eccentric rotor in an electrical machine have been discussed for more than one hundred years [1], and the beneficial effects of parallel windings in mitigating the resultant UMP have been discussed almost as long [2]. It is common practice for manufacturers to use parallel stator windings in motors because these are well known to reduce the motor noise, vibration and UMP [3, 4]. Moreover, the parallel connections also often simplify the manufacturing of the stator winding in large machines. The rotor cage (or damper winding) is also capable of effectively attenuating the force associated with rotor eccentricity [5].

Traditionally, analytical approaches were used to study the operation of electrical machines with eccentric rotors [3, 6]. Later, numerical methods have also been employed to study the UMP reduction by the currents circulating in the parallel paths of the stator and rotor windings [7].

Using the permeance harmonic analysis presented by Früchtenicht *et al.* [8], Arkkio *et al.* [9] developed a low-order model to represent the electromagnetic force acting on an eccentric rotor of an induction machine equipped only with the rotor cage (no parallel stator windings). The force model was not restricted to special cases of static and/or dynamic eccentricities, as in most of the previously published work, but instead described the UMP in a wide whirling frequency range. In [10], Burakov and Arkkio presented a force model for a salient-pole synchronous machine equipped with the rotor cage. A parametric force model for electrical machines with parallel stator windings was presented in [11]. This model performed very well when applied to a salient-pole synchronous machine and also to an induction machine, which both did not have the rotor cage.

This paper continues the previous work and puts forward a parametric model to describe the UMP in an eccentric-rotor electrical machine, which has both the rotor cage and parallel stator windings. The model is originally targeted at a salient-pole synchronous machine, but, as will be shown hereafter, it also works fine with an induction machine. The force model accounts for the effects of the equalising currents flowing in the parallel paths of the stator and rotor windings. Moreover, the coupling between the stator and rotor equalising currents is also included in the model. Force model parameters are estimated from the numerical test results, where the effects of iron core saturation, stator and rotor slotting are all taken into account. The model with estimated parameters shows an accurate performance in a wide whirling frequency range. The force model proposed has the following advantages:

1. It allows simple, quick and accurate calculation of the electromagnetic force at a desired whirling frequency value or in a certain range of whirling frequencies;
2. The same model parameters can be directly used at different values of whirling radius and whirling frequency;

doi:10.1049/iet-epa:20060227

Paper first received 9th June and in revised form 26th October 2006

The authors are with the Helsinki University of Technology, Laboratory of Electromechanics, PO Box 3000, FIN-02015 HUT, Finland

E-mail: andrej.burakov@tkk.fi

3. The model offers an attractive opportunity to be integrated into the mechanical analysis to study the electromechanical interactions in electrical machines;
4. The model performs accurately when applied to synchronous and induction machines; no changes are needed in the model expression. Moreover, the model performs also very well when used with electrical machines equipped with either the parallel stator windings or the rotor cage.

However there is a necessity to re-estimate the force model parameters every time the operating point (supply voltage, load torque etc.) of a machine is changed.

2 Methods of analysis

In this work, a salient-pole synchronous machine operating in steady state was studied, therefore the fundamental component of the magnetic flux density was assumed to be constant and unaffected by the rotor eccentricity. Only the cylindrical circular rotor whirling was considered, meaning that the rotor axis, when travelling at a circular orbit around the stator bore axis, remained always parallel to it. Instead of resorting to the classical two-axis approach, a vector representation for the machine quantities was used, which allowed for a considerably improved clarity, conciseness and simplicity of the resultant expressions.

The cross-section view of the machine studied is shown in Fig. 1. The stator and rotor axes were assumed to be perpendicular to the plane of the figure and the magnetic field in the core region was assumed to be two-dimensional and parallel to this plane. Although the field winding magnetomotive force (MMF) in a salient-pole synchronous machine is constant within the angular length of a rotor pole, hereafter we used the sinusoidal distribution of the MMF. This assumption simplified the magnetic field analysis and had almost no effect on the spatial distribution of the resultant magnetic flux density in the air gap. More details on this simplification are given in Section 2.1.

The machine studied was equipped with four parallel stator windings, connected in such a way that the neighbouring pole windings were in series and the opposite pole windings were in parallel. Motors incorporating this kind of stator winding were reported to run more quietly than those with neighbouring pole windings in parallel and the opposite pole windings in series [7].

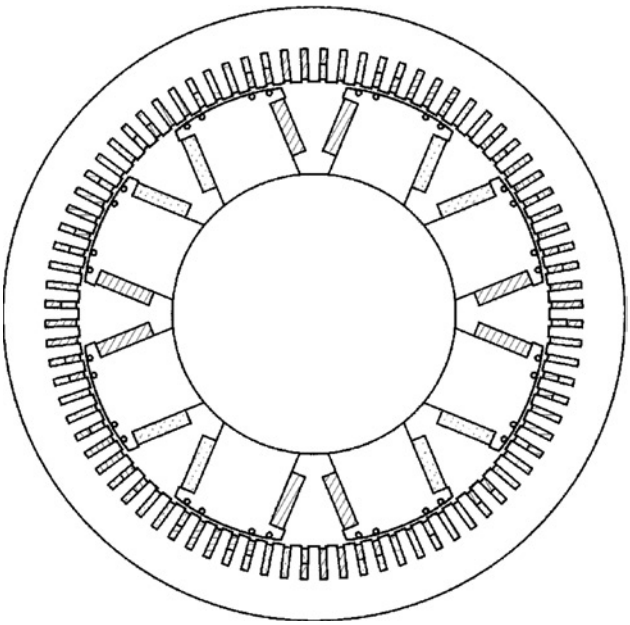

Fig. 1 *Cross-section view of synchronous machine studied*

Each rotor pole shoe comprised four damper bars made of copper, which were short-circuited by end rings. The parallel paths of the field winding, which were expected to have the UMP reduction effects similar to those by the rotor cage, were not considered in this work.

2.1 Magnetomotive forces

The resultant MMF of the machine studied consisted of MMFs produced by the field (rotor), armature (stator) and damper windings.

The field winding was concentrated on the rotor poles, therefore the MMF spectrum of this winding contained several harmonics. For the eight-pole machine studied, the five most prominent field winding MMF components and their values relative to the fundamental MMF component are listed in Table 1. These data were obtained from the analytical model of the machine, wherein the rotor saliency was accounted for.

As seen, the fundamental component of the field winding MMF is preponderant. As for the stator winding MMF, the supremacy of the fundamental component was expected to be even greater, because the winding was distributed along the stator bore circumference. Hence, in the following, only the fundamental MMF component is considered. This simplification was also used in [12], where a general model for the analysis of a salient-pole machine, as well as for a nonsalient-pole machine was developed.

The field winding rotates with the rotor, thus its MMF can be expressed as

$$F_{\mathrm{f}}^{\mathrm{s}}(\varphi, t) = \mathrm{Re}\left\{\left(\frac{N_{\mathrm{f}}}{2p} i_{\mathrm{f}}\right) \mathrm{e}^{\mathrm{j}(p\varphi - \omega_1 t)}\right\} = \mathrm{Re}\left\{F_{\mathrm{f},p} \mathrm{e}^{\mathrm{j}(p\varphi - \omega_1 t)}\right\} \tag{1}$$

where, p indicates the number of pole pairs and the corresponding wave number; N_{f} is the number of field winding turns in series; i_{f} is field winding current; $\omega_1 = p\Omega_{\mathrm{m}}$ (in the general case, $\Omega_{\mathrm{m}} = (1 - s)\omega_1/p$, s is slip) is the angular speed of the stator supply voltage; Ω_{m} is the mechanical angular velocity of the rotor; φ is the angular co-ordinate; t denotes time; superscript 's' indicate that a stator reference frame is used. Hereafter, a general expression for Ω_{m} has been used ($s \neq 0$), as the force model elaborated in this work was also applied to an induction machine.

As already mentioned, currents supplied to the stator winding from the mains were assumed to have sinusoidal spatial distribution. Besides that, the parallel stator windings provided paths for the circulating currents, due to numerous magnetic flux harmonics present in the air gap. Those having nonzero winding factors would generate the

Table 1: Content of field winding MMF spectrum

Harmonic (Number of pole pairs)	Relative magnitude
4	1
12	0.199
20	0.016
28	0.030
36	0.02

corresponding MMF harmonics

$$F_{\mathrm{s}}^{\mathrm{s}}(\varphi, t) = \sum_{k=1}^{N_1} \mathrm{Re}\left\{\left(\frac{3}{2}\frac{N_{\mathrm{se},k}}{2p} i_k\right) \mathrm{e}^{\mathrm{j}(k\varphi - \omega_k t + \varphi_{\mathrm{s},k})}\right\}$$

$$= \sum_{k=1}^{N_1} \mathrm{Re}\left\{F_{\mathrm{s},k} \mathrm{e}^{\mathrm{j}(k\varphi - \omega_k t + \varphi_{\mathrm{s},k})}\right\} \quad (2)$$

where k is the wave number of the MMF harmonic; N_1 is the highest considered harmonic of the stator MMF, $N_{\mathrm{se},k} = 4k_{\mathrm{sw},k}N_{\mathrm{s}}/\pi$ is the equivalent number of the stator winding turns in series for the kth stator current harmonic; $k_{\mathrm{sw},k}$ is the winding factor for the corresponding stator current harmonic; N_{s} is the number of stator winding turns in series; i_k is the stator current harmonic which causes the MMF harmonic with wave number k; $\varphi_{\mathrm{s},k}$ is phase angle of the kth MMF harmonic with respect to the field winding MMF.

Note that a current induced in a single parallel circuit of the stator winding by a magnetic flux passing through it can only produce a standing MMF wave, however, when interacting with currents induced in other parallel windings, it can cause the travelling MMF harmonics with different wave numbers.

As this study was primarily concerned with the steady-state operation of a synchronous machine, the fundamental MMF component produced by the damper winding was presumed to be absent. This assumption was justified by the fact that, in a synchronous machine operating in a steady-state mode, the fundamental magnetic field component passing through the damper winding has a constant magnitude and is stationary with respect to the winding. Thus, there are no fundamental electromotive forces induced in the damper winding, no fundamental currents and, hence, no fundamental MMF produced by this winding. By taking into account the other components of the damper winding current, we have

$$F_{\mathrm{r},n}^{\mathrm{s}}(\varphi, t) = \sum_{\substack{n=1 \\ n\neq p}}^{N_2} \mathrm{Re}\left\{k_{\mathrm{sw},n} i_{\mathrm{r},n} \mathrm{e}^{\mathrm{j}(n\varphi - \omega_n t + \varphi_{\mathrm{r},n})}\right\}$$

$$= \sum_{\substack{n=1 \\ n\neq p}}^{N_2} \mathrm{Re}\left\{F_{\mathrm{r},n} \mathrm{e}^{\mathrm{j}(n\varphi - \omega_n t + \varphi_{\mathrm{r},n})}\right\} \quad (3)$$

where n is the wave number of the MMF harmonic; N_2 is the highest considered harmonic of the MMF produced by the damper winding; $k_{\mathrm{sw},n}$ is the winding factor for the corresponding damper winding harmonic; $\varphi_{\mathrm{r},n}$ is phase angle of nth MMF harmonic with respect to the field winding MMF.

The net MMF is the sum of the field, stator and damper winding MMFs

$$F^{\mathrm{s}}(\varphi, t) = \mathrm{Re}\left\{(F_{\mathrm{f},p} + F_{\mathrm{s},p}\mathrm{e}^{\mathrm{j}\varphi_{\mathrm{s},p}})\mathrm{e}^{\mathrm{j}(p\varphi - \omega_1 t)}\right.$$

$$+ \sum_{\substack{k=1, \\ k\neq p}}^{N_1} F_{\mathrm{s},k} \mathrm{e}^{\mathrm{j}(k\varphi - \omega_k t + \varphi_{\mathrm{s},k})}$$

$$\left. + \sum_{\substack{n=1 \\ n\neq p}}^{N_2} F_{\mathrm{r},n} \mathrm{e}^{\mathrm{j}(n\varphi - \omega_n t + \varphi_{\mathrm{r},n})}\right\} \quad (4)$$

As it was already mentioned before, the MMF of the field winding is not sinusoidally distributed but rather constant over the rotor pole. On the other hand, the air-gap length over the pole shoe is varying and so is the air gap permeance. This is done to achieve a sinusoidal distribution of the magnetic flux density produced by the field winding. When deriving the parametric force model, we have used a sinusoidal distribution of the field winding MMF and a constant air gap (if no eccentricity is present), instead of the actual constant MMF and varying air-gap length. It can be shown that both approaches provide very similar distributions of the magnetic flux density in the air gap.

2.2 Air-gap permeance

In [13], it was shown that the circumferential air-gap variation in a salient-pole synchronous machine with concentric rotor can be expressed as

$$\delta^{\mathrm{s}}(\varphi, t) = \mathrm{Re}\left\{\frac{\delta_{0\,\min}}{\left|\cos((\pi/\tau)\varphi)\right|} \mathrm{e}^{-\mathrm{j}2\omega_1 t}\right\} \quad (5)$$

where $\pi_{\min}$ is the smallest air gap between the rotor pole shoe and the stator surface (on the pole axis); τ is the pole pitch $\tau = \pi/p$; || denotes an absolute value.

Equation (5) can also be written as

$$\delta^{\mathrm{s}}(\varphi, t) = \mathrm{Re}\left\{\frac{\delta_{0\,\min}}{\left|\cos(p\varphi)\right|} \mathrm{e}^{-\mathrm{j}2\omega_1 t}\right\} \quad (6)$$

Cylindrical rotor whirling causes an additional term in the air gap expression

$$\delta^{\mathrm{s}}(\varphi, t) = \mathrm{Re}\left\{\frac{\delta_{0\,\min}}{\left|\cos(p\varphi)\right|} \mathrm{e}^{-\mathrm{j}2\omega_1 t} + \delta_{\mathrm{ecc}} \mathrm{e}^{\mathrm{j}(\varphi - \omega_{\mathrm{ecc}} t + \varphi_{\mathrm{ecc.0}})}\right\} \quad (7)$$

where δ_{ecc} is whirling radius; ω_{ecc} is whirling angular speed; $\varphi_{\mathrm{ecc.0}}$ is the initial phase angle of the rotor eccentricity.

The air-gap permeance was calculated as

$$\lambda^{\mathrm{s}}(\varphi, t) = \frac{\mu_0}{\delta^{\mathrm{s}}(\varphi, t)} \quad (8)$$

where μ_0 is permeability of free space.

Substituting (7) into (8) resulted in a Fourier series where the most prominent components had wave numbers 0, 1 and $2p$

$$\lambda^{\mathrm{s}}(\varphi, t) = \frac{\mu_0}{\delta_0}\left(1 + \frac{1}{\delta_0}\mathrm{Re}\left\{\delta_{\mathrm{ecc}} \mathrm{e}^{\mathrm{j}(\varphi - \omega_{\mathrm{ecc}} t + \varphi_{\mathrm{ecc.0}})}\right\}\right.$$

$$\left. + \frac{1}{\delta_0}\mathrm{Re}\left\{\delta_{\mathrm{ps}} \mathrm{e}^{\mathrm{j}(2p\varphi - 2\omega_1 t)}\right\}\right) \quad (9)$$

where δ_0 is the constant term of the Fourier series, which also accounts for the fictitious air gap increase due to saturation, $\delta_{\mathrm{ps}}\mathrm{e}^{\mathrm{j}(2p\varphi - 2\omega_1 t)}$ is the first Fourier component associated with rotor saliency.

Results of the analytical simulation based on (5)–(8) for an eight-pole machine are presented in Fig. 2, where the rotor eccentricity value was 20% of the air gap $\delta_{0\,\min}$. As seen, the constant permeance term and those associated with rotor saliency and rotor eccentricity are preponderant. These observations agree with (9).

2.3 Magnetic flux density

The magnetic flux density in the air gap was obtained as a product of MMF and permeance

$$B^{\mathrm{s}}(\varphi, t) = F^{\mathrm{s}}(\varphi, t) \cdot \lambda^{\mathrm{s}}(\varphi, t) \quad (10)$$

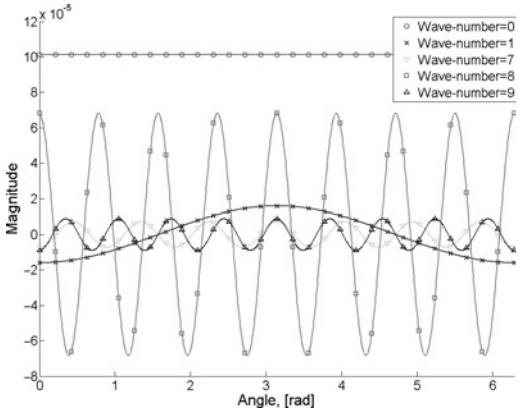

Fig. 2 *Air-gap permeance waves for eight-pole synchronous machine*

Substituting (4) and (9) into (10), we have the following

$$
\begin{aligned}
&B^{\mathrm{s}}(\varphi,t)\\
&=\frac{\mu_0}{\delta_0}\mathrm{Re}\Bigg\{\Bigg[\left(F_{\mathrm{f},p}+F_{\mathrm{s},p}\mathrm{e}^{\mathrm{j}\varphi_{\mathrm{s},p}}\right)\mathrm{e}^{-\mathrm{j}\omega_1 t}\\
&+\frac{\delta_{\mathrm{ps}}}{2\delta_0}\Bigg(\left(F_{\mathrm{f},p}+F_{\mathrm{s},p}\mathrm{e}^{-\mathrm{j}\varphi_{\mathrm{s},p}}\right)\mathrm{e}^{-\mathrm{j}\omega_1 t}\\
&+\left(F_{\mathrm{s},3p}\mathrm{e}^{\mathrm{j}\varphi_{\mathrm{s},3p}}+F_{\mathrm{r},3p}\mathrm{e}^{\mathrm{j}\varphi_{\mathrm{r},3p}}\right)\mathrm{e}^{-\mathrm{j}(\omega_{3p}-2\omega_1)t}\Bigg)\\
&+\frac{\delta_{\mathrm{ecc}}}{2\delta_0}\Bigg(\left(F_{\mathrm{s},p\pm1}\mathrm{e}^{\mathrm{j}\varphi_{\mathrm{s},p\pm1}}+F_{\mathrm{r},p\pm1}\mathrm{e}^{\mathrm{j}\varphi_{\mathrm{r},p\pm1}}\right)\\
&\times\mathrm{e}^{-\mathrm{j}\left((\omega_{p\pm1}\mp\omega_{\mathrm{ecc}})t\pm\varphi_{\mathrm{ecc}.0}\right)}\Bigg)\Bigg]\mathrm{e}^{\mathrm{j}p\varphi}\\
&+\Bigg[\left(F_{\mathrm{s},p-1}\mathrm{e}^{\mathrm{j}\varphi_{\mathrm{s},p-1}}+F_{\mathrm{r},p-1}\mathrm{e}^{\mathrm{j}\varphi_{\mathrm{r},p-1}}\right)\mathrm{e}^{-\mathrm{j}\omega_{p-1}t}\\
&+\frac{\delta_{\mathrm{ps}}}{2\delta_0}\Bigg(\left(F_{\mathrm{s},3p-1}\mathrm{e}^{\mathrm{j}\varphi_{\mathrm{s},3p-1}}+F_{\mathrm{r},3p-1}\mathrm{e}^{\mathrm{j}\varphi_{\mathrm{r},3p-1}}\right)\mathrm{e}^{-\mathrm{j}(\omega_{3p-1}-2\omega_1)t}\\
&+\left(F_{\mathrm{s},p+1}\mathrm{e}^{\mathrm{j}\varphi_{\mathrm{s},p+1}}+F_{\mathrm{r},p+1}\mathrm{e}^{\mathrm{j}\varphi_{\mathrm{r},p+1}}\right)\mathrm{e}^{\mathrm{j}(\omega_{p+1}-2\omega_1)t}\Bigg)\\
&+\frac{\delta_{\mathrm{ecc}}}{2\delta_0}\left(F_{\mathrm{f},p}+F_{\mathrm{s},p}\mathrm{e}^{\mathrm{j}\varphi_{\mathrm{s},p}}\right)\mathrm{e}^{-\mathrm{j}((\omega_1-\omega_{\mathrm{ecc}})t+\varphi_{\mathrm{ecc}.0})}\Bigg]\mathrm{e}^{\mathrm{j}(p-1)\varphi}\\
&+\Bigg[\left(F_{\mathrm{s},p+1}\mathrm{e}^{\mathrm{j}\varphi_{\mathrm{s},p+1}}+F_{\mathrm{r},p+1}\mathrm{e}^{\mathrm{j}\varphi_{\mathrm{r},p+1}}\right)\mathrm{e}^{-\mathrm{j}\omega_{p+1}t}\\
&+\frac{\delta_{\mathrm{ps}}}{2\delta_0}\Bigg(\left(F_{\mathrm{s},3p+1}\mathrm{e}^{\mathrm{j}\varphi_{\mathrm{s},3p+1}}+F_{\mathrm{r},3p+1}\mathrm{e}^{\mathrm{j}\varphi_{\mathrm{r},3p+1}}\right)\mathrm{e}^{-\mathrm{j}(\omega_{3p+1}-2\omega_1)t}\\
&+\left(F_{\mathrm{s},p-1}\mathrm{e}^{\mathrm{j}\varphi_{\mathrm{s},p-1}}+F_{\mathrm{r},p-1}\mathrm{e}^{\mathrm{j}\varphi_{\mathrm{r},p-1}}\right)\mathrm{e}^{\mathrm{j}(\omega_{p-1}-2\omega_1)t}\Bigg)\\
&+\frac{\delta_{\mathrm{ecc}}}{2\delta_0}\left(F_{\mathrm{f},p}+F_{\mathrm{s},p}\mathrm{e}^{\mathrm{j}\varphi_{\mathrm{s},p}}\right)\mathrm{e}^{-\mathrm{j}\left((\omega_1+\omega_{\mathrm{ecc}})t-\varphi_{\mathrm{ecc}.0}\right)}\Bigg]\mathrm{e}^{\mathrm{j}(p+1)\varphi}\\
&+\sum_{\substack{k=1,\\k\neq p,p\pm1}}^{N_1}F_{\mathrm{s},k}\mathrm{e}^{\mathrm{j}(k\varphi-\omega_k t+\varphi_{\mathrm{s},k})}+\sum_{\substack{n=1\\n\neq p,p\pm1}}^{N_2}F_{\mathrm{r},n}\mathrm{e}^{\mathrm{j}(n\varphi-\omega_n t+\varphi_{\mathrm{r},n})}\\
&+\frac{\delta_{\mathrm{ecc}}}{2\delta_0}\Bigg(\left(F_{\mathrm{s},p\pm1}\mathrm{e}^{\mathrm{j}\varphi_{\mathrm{s},p\pm1}}+F_{\mathrm{r},p\pm1}\mathrm{e}^{\mathrm{j}\varphi_{\mathrm{r},p\pm1}}\right)\\
&\times\mathrm{e}^{\mathrm{j}\left((p\pm2)\varphi-(\omega_{p\pm1}\pm\omega_{\mathrm{ecc}})t\pm\varphi_{\mathrm{ecc}.0}\right)}\\
&+\sum_{\substack{k=1,\\k\neq p,p\pm1}}^{N_1}F_{\mathrm{s},k}\mathrm{e}^{\mathrm{j}\left((k\pm1)\varphi-(\omega_k\pm\omega_{\mathrm{ecc}})t+\varphi_{\mathrm{s},k}\pm\varphi_{\mathrm{ecc}.0}\right)}\\
&+\sum_{\substack{n=1\\n\neq p,p\pm1}}^{N_2}F_{\mathrm{r},n}\mathrm{e}^{\mathrm{j}\left((n\pm1)\varphi-(\omega_n\pm\omega_{\mathrm{ecc}})t+\varphi_{\mathrm{r},n}\pm\varphi_{\mathrm{ecc}.0}\right)}\Bigg)\\
&+\frac{\delta_{\mathrm{ps}}}{2\delta_0}\Bigg(\left(F_{\mathrm{f},p}+F_{\mathrm{s},p}\mathrm{e}^{\mathrm{j}\varphi_{\mathrm{s},p}}\right)\mathrm{e}^{\mathrm{j}(3p\varphi-3\omega_1 t)}\\
&+\left(F_{\mathrm{s},p\pm1}\mathrm{e}^{\mathrm{j}\varphi_{\mathrm{s},p\pm1}}+F_{\mathrm{r},p\pm1}\mathrm{e}^{\mathrm{j}\varphi_{\mathrm{r},p\pm1}}\right)\mathrm{e}^{\mathrm{j}\left((3p\pm1)\varphi-(\omega_{p\pm1}+2\omega_1)t\right)}\\
&+\left(F_{\mathrm{s},3p}\mathrm{e}^{\mathrm{j}\varphi_{\mathrm{s},3p}}+F_{\mathrm{r},3p}\mathrm{e}^{\mathrm{j}\varphi_{\mathrm{r},3p}}\right)\mathrm{e}^{\mathrm{j}\left(5p\varphi-(\omega_{3p}+2\omega_1)t\right)}\\
&+\left(F_{\mathrm{s},3p\pm1}\mathrm{e}^{\mathrm{j}\varphi_{\mathrm{s},3p\pm1}}+F_{\mathrm{r},3p\pm1}\mathrm{e}^{\mathrm{j}\varphi_{\mathrm{r},3p\pm1}}\right)\\
&\times\mathrm{e}^{\mathrm{j}\left((5p\pm1)\varphi-(\omega_{3p\pm1}+2\omega_1)t\right)}\\
&+\sum_{\substack{k=1,\\k\neq p,p\pm1,3p,3p\pm1}}^{N_1}F_{\mathrm{s},k}\mathrm{e}^{\mathrm{j}\left((k\pm2p)\varphi-(\omega_k\pm2\omega_1)t+\varphi_{\mathrm{s},k}\right)}\\
&+\sum_{\substack{n=1\\n\neq p,p\pm1,3p,3p\pm1}}^{N_2}F_{\mathrm{r},n}\mathrm{e}^{\mathrm{j}((n\pm2p)\varphi-(\omega_n\pm2\omega_1)t+\varphi_{\mathrm{r},n})}\Bigg)\Bigg\}
\end{aligned}
\tag{11a}
$$

In this equation, it is interesting to observe that the $p-1$ magnetic flux density harmonic can be produced by the interaction of $p+1$ MMF harmonics with the permeance wave due to the rotor saliency (note the term $\delta_{\mathrm{ps}}/2\delta_0\left(F_{\mathrm{s},p+1}\mathrm{e}^{\mathrm{j}\varphi_{\mathrm{s},p+1}}+F_{\mathrm{r},p+1}\mathrm{e}^{\mathrm{j}\varphi_{\mathrm{r},p+1}}\right)\mathrm{e}^{\mathrm{j}((p-1)\varphi+(\omega_{p+1}-2\omega_1)t)}$). Similarly, the product of $p-1$ MMF harmonics and the same permeance wave can generate a magnetic flux density harmonic with wave number $p+1$ (term $\delta_{\mathrm{ps}}/2\delta_0(F_{\mathrm{s},p-1}\mathrm{e}^{\mathrm{j}\varphi_{\mathrm{s},p-1}}+F_{\mathrm{r},p-1}\mathrm{e}^{\mathrm{j}\varphi_{\mathrm{r},p-1}})\ \mathrm{e}^{\mathrm{j}((p+1)\varphi+(\omega_{p-1}-2\omega_1)t)}$). Though these constituents of $p\pm1$ magnetic flux density terms are expected to be small and neglected hereafter, they show that there can be a coupling between the two magnetic flux density harmonics, commonly known as eccentricity harmonics.

Rotor eccentricity engenders mainly the magnetic flux density terms having wave numbers $p\pm1$. These, interacting with the fundamental field, will generate the UMP. Hence, by taking into account only the strongest magnetic flux density components, (11a) can be reduced to

$$
\begin{aligned}
B^{\mathrm{s}}(\varphi,t)=\frac{\mu_0}{\delta_0}\mathrm{Re}\Bigg\{&\Bigg[\left(F_{\mathrm{f},p}+F_{\mathrm{s},p}\mathrm{e}^{\mathrm{j}\varphi_{\mathrm{s},p}}\right)\mathrm{e}^{-\mathrm{j}\omega_1 t}\\
&+\frac{\delta_{\mathrm{ps}}}{2\delta_0}\left(F_{\mathrm{f},p}+F_{\mathrm{s},p}\mathrm{e}^{-\mathrm{j}\varphi_{\mathrm{s},p}}\right)\mathrm{e}^{-\mathrm{j}\omega_1 t}\Bigg]\mathrm{e}^{\mathrm{j}p\varphi}\\
&+\Bigg[\frac{\delta_{\mathrm{ecc}}}{2\delta_0}\left(F_{\mathrm{f},p}+F_{\mathrm{s},p}\mathrm{e}^{\mathrm{j}\varphi_{\mathrm{s},p}}\right)\mathrm{e}^{-\mathrm{j}\left((\omega_1-\omega_{\mathrm{ecc}})t+\varphi_{\mathrm{ecc}.0}\right)}\\
&+\left(F_{\mathrm{s},p-1}\mathrm{e}^{\mathrm{j}\varphi_{\mathrm{s},p-1}}+F_{\mathrm{r},p-1}\mathrm{e}^{\mathrm{j}\varphi_{\mathrm{r},p-1}}\right)\mathrm{e}^{-\mathrm{j}\omega_{p-1}t}\Bigg]\mathrm{e}^{\mathrm{j}(p-1)\varphi}\\
&+\Bigg[\frac{\delta_{\mathrm{ecc}}}{2\delta_0}\left(F_{\mathrm{f},p}+F_{\mathrm{s},p}\mathrm{e}^{\mathrm{j}\varphi_{\mathrm{s},p}}\right)\mathrm{e}^{-\mathrm{j}\left((\omega_1+\omega_{\mathrm{ecc}})t-\varphi_{\mathrm{ecc}.0}\right)}\\
&+\left(F_{\mathrm{s},p+1}\mathrm{e}^{\mathrm{j}\varphi_{\mathrm{s},p+1}}+F_{\mathrm{r},p+1}\mathrm{e}^{\mathrm{j}\varphi_{\mathrm{r},p+1}}\right)\mathrm{e}^{-\mathrm{j}\omega_{p+1}t}\Bigg]\mathrm{e}^{\mathrm{j}(p+1)\varphi}\Bigg\}
\end{aligned}
\tag{11b}
$$

Equation (11b) can be rewritten as

$$B^{\mathrm{s}}(\varphi,t)=\mathrm{Re}\left\{\underline{B}^{\mathrm{s}}_{p}\mathrm{e}^{\mathrm{j}p\varphi}+\underline{B}^{\mathrm{s}}_{p-1}\mathrm{e}^{\mathrm{j}(p-1)\varphi}+\underline{B}^{\mathrm{s}}_{p+1}\mathrm{e}^{\mathrm{j}(p+1)\varphi}\right\} \quad (12)$$

where bar underlining a quantity means that the corresponding quantity is complex-valued. In this work, the complex notation was employed to denote the time dependence of the corresponding variables, if it is not stated otherwise. The shortening notations in (12) are

$$\begin{aligned}
\underline{B}^{\mathrm{s}}_{p}&=\frac{\mu_0}{\delta_0}\left[\left(F_{\mathrm{f},p}+F_{\mathrm{s},p}\mathrm{e}^{\mathrm{j}\varphi_{\mathrm{s},p}}\right)\right.\\
&\quad\left.+\frac{\delta_{\mathrm{ps}}}{2\delta_0}\left(F_{\mathrm{f},p}+F_{\mathrm{s},p}\mathrm{e}^{-\mathrm{j}\varphi_{\mathrm{s},p}}\right)\right]\mathrm{e}^{-\mathrm{j}\omega_1 t}\\
\underline{B}^{\mathrm{s}}_{p-1}&=\frac{\mu_0}{\delta_0}\left[\frac{\delta_{\mathrm{ecc}}}{2\delta_0}\left(F_{\mathrm{f},p}+F_{\mathrm{s},p}\mathrm{e}^{\mathrm{j}\varphi_{\mathrm{s},p}}\right)\mathrm{e}^{-\mathrm{j}((\omega_1-\omega_{\mathrm{ecc}})t+\varphi_{\mathrm{ecc.0}})}\right.\\
&\quad\left.+\left(F_{\mathrm{s},p-1}\mathrm{e}^{\mathrm{j}\varphi_{\mathrm{s},p-1}}+F_{\mathrm{r},p-1}\mathrm{e}^{\mathrm{j}\varphi_{\mathrm{r},p-1}}\right)\mathrm{e}^{-\mathrm{j}\omega_{p-1}t}\right]\\
\underline{B}^{\mathrm{s}}_{p+1}&=\frac{\mu_0}{\delta_0}\left[\frac{\delta_{\mathrm{ecc}}}{2\delta_0}\left(F_{\mathrm{f},p}+F_{\mathrm{s},p}\mathrm{e}^{\mathrm{j}\varphi_{\mathrm{s},p}}\right)\mathrm{e}^{-\mathrm{j}(\omega_1+\omega_{\mathrm{ecc}})t-\varphi_{\mathrm{ecc.0}}}\right.\\
&\quad\left.+\left(F_{\mathrm{s},p+1}\mathrm{e}^{\mathrm{j}\varphi_{\mathrm{s},p+1}}+F_{\mathrm{r},p+1}\mathrm{e}^{\mathrm{j}\varphi_{\mathrm{r},p+1}}\right)\mathrm{e}^{-\mathrm{j}\omega_{p+1}t}\right]
\end{aligned} \quad (13)$$

Equations (13) can also be written in another form, wherein the $p\pm1$ magnetic flux densities are expressed in terms of the fundamental field and corresponding currents in the stator and rotor windings

$$\begin{aligned}
\underline{B}^{\mathrm{s}}_{p}&=\left(B_{p,1}\mathrm{e}^{\mathrm{j}\varphi_p}+B_{p,2}\mathrm{e}^{-\mathrm{j}\varphi_p}\right)\mathrm{e}^{-\mathrm{j}\omega_1 t}\\
\underline{B}^{\mathrm{s}}_{p-1}&=\frac{\delta_{\mathrm{ecc}}}{2\delta_0}B_{p,1}\mathrm{e}^{-\mathrm{j}((\omega_1-\omega_{\mathrm{ecc}})t-\varphi_p+\varphi_{\mathrm{ecc.0}})}\\
&\quad+\frac{\mu_0}{\delta_0}\left(k_{\mathrm{cs},p-1}\underline{i}^{\mathrm{s}}_{\mathrm{s},p-1}+k_{\mathrm{cr},p-1}\underline{i}^{\mathrm{s}}_{\mathrm{r},p-1}\right)\\
\underline{B}^{\mathrm{s}}_{p+1}&=\frac{\delta_{\mathrm{ecc}}}{2\delta_0}B_{p,1}\mathrm{e}^{-\mathrm{j}((\omega_1+\omega_{\mathrm{ecc}})t-\varphi_p-\varphi_{\mathrm{ecc.0}})}\\
&\quad+\frac{\mu_0}{\delta_0}\left(k_{\mathrm{cs},p+1}\underline{i}^{\mathrm{s}}_{\mathrm{s},p+1}+k_{\mathrm{cr},p+1}\underline{i}^{\mathrm{s}}_{\mathrm{r},p+1}\right)
\end{aligned} \quad (14)$$

where $B_{p,1}$ is caused by the interaction of the fundamental MMF components and constant permeance term; $B_{p,2}$ is the product of the fundamental MMF components with the first Fourier-series component of the air-gap permeance related to rotor saliency; φ_p accounts for the phase angle shift of the magnetic-flux-density harmonics with respect to the MMF vector of the field winding; $k_{\mathrm{cs},p\pm1}$ and $k_{\mathrm{cr},p\pm1}$ are dimensionless coupling factors related to the stator and rotor windings, respectively.

2.4 Magnetic fluxes through the stator and rotor windings

In the rotor frame of reference, the $p\pm1$ magnetic field waves through the damper winding can be expressed as

$$\begin{aligned}
\underline{\phi}^{\mathrm{r}}_{\mathrm{r},p-1}&=L_{\mathrm{self,r},p-1}\underline{i}^{\mathrm{r}}_{\mathrm{r},p-1}+k_{\mathrm{L,r},p-1}\\
&\quad\times\left(\frac{\delta_{\mathrm{ecc}}}{2\mu_0}B_{p,1}\mathrm{e}^{-\mathrm{j}((s\omega_1-\omega^{\mathrm{r}}_{\mathrm{ecc}})t-\varphi_p+\varphi_{\mathrm{ecc.0}})}+k_{\mathrm{cs},p-1}\underline{i}^{\mathrm{r}}_{\mathrm{s},p-1}\right)\\
\underline{\phi}^{\mathrm{r}}_{\mathrm{r},p+1}&=L_{\mathrm{self,r},p+1}\underline{i}^{\mathrm{r}}_{\mathrm{r},p+1}+k_{\mathrm{L,r},p+1}\\
&\quad\times\left(\frac{\delta_{\mathrm{ecc}}}{2\mu_0}B_{p,1}\mathrm{e}^{-\mathrm{j}((s\omega_1+\omega^{\mathrm{r}}_{\mathrm{ecc}})t-\varphi_p-\varphi_{\mathrm{ecc.0}})}+k_{\mathrm{cs},p+1}\underline{i}^{\mathrm{r}}_{\mathrm{s},p+1}\right)
\end{aligned} \quad (15)$$

where $\omega^{\mathrm{r}}_{\mathrm{ecc}}$ is whirling angular speed in the rotor reference frame ($\omega^{\mathrm{r}}_{\mathrm{ecc}}=\omega_{\mathrm{ecc}}-\Omega_{\mathrm{m}}$), coefficients $k_{\mathrm{L,r},p\pm1}$ have the unit of henry (H) and define the amounts of the corresponding magnetic flux harmonics that pass through the damper winding from the sources other than rotor currents, $L_{\mathrm{self,r},p\pm1}$ are self-inductances of the damper winding for the corresponding magnetic field waves. According to [8], the self-inductances are defined as

$$L_{\mathrm{self,r},p\pm1}=\mu_0\frac{\pi d_{\mathrm{r}}l_{\mathrm{e}}K_{\mathrm{w},p\pm1}}{Z_{\mathrm{bars}}\delta_{\mathrm{e}}}$$

where d_{r} is the diameter of the damper winding, l_{e} is equivalent axial length of the damper winding, $K_{\mathrm{w},p\pm1}$ are winding factors for the corresponding harmonics, Z_{bars} is number of damper bars and δ_{e} is equivalent air gap including the effect of slotting.

Similarly, the magnetic-flux harmonics linking the stator winding can be expressed as

$$\begin{aligned}
\underline{\psi}^{\mathrm{s}}_{\mathrm{s},p-1}&=L_{\mathrm{self,s},p-1}\underline{i}^{\mathrm{s}}_{\mathrm{s},p-1}+k_{\mathrm{L,s},p-1}\\
&\quad\times\left(\frac{\delta_{\mathrm{ecc}}}{2\mu_0}B_{p,1}\mathrm{e}^{-\mathrm{j}((\omega_1-\omega_{\mathrm{ecc}})t-\varphi_p+\varphi_{\mathrm{ecc.0}})}+k_{\mathrm{cr},p-1}\underline{i}^{\mathrm{s}}_{\mathrm{r},p-1}\right)\\
\underline{\psi}^{\mathrm{s}}_{\mathrm{s},p+1}&=L_{\mathrm{self,s},p+1}\underline{i}^{\mathrm{s}}_{\mathrm{s},p+1}+k_{\mathrm{L,s},p+1}\\
&\quad\times\left(\frac{\delta_{\mathrm{ecc}}}{2\mu_0}B_{p,1}\mathrm{e}^{-\mathrm{j}((\omega_1+\omega_{\mathrm{ecc}})t-\varphi_p-\varphi_{\mathrm{ecc.0}})}+k_{\mathrm{cr},p+1}\underline{i}^{\mathrm{s}}_{\mathrm{r},p+1}\right)
\end{aligned} \quad (16)$$

where $L_{\mathrm{self,r},p\pm1}$ are self-inductances of the stator winding for the corresponding magnetic field waves, coefficients $k_{\mathrm{L,s},p\pm1}$ define the amounts of the corresponding magnetic flux harmonics that pass through the stator winding from the sources other than stator currents. Note that in (16) the stator reference frame was used.

2.5 Voltage equations for the stator and rotor windings

The damper winding can be considered as a number of loops consisting of two neighbouring bars short-circuited by the end rings. Owing to the short-circuit, the voltages induced by the $p\pm1$ magnetic field harmonics in each loop vanish

$$\begin{aligned}
\left(R_{\mathrm{r},p-1}+L_{\acute{\mathrm{o}}\mathrm{r},p-1}\frac{\mathrm{d}}{\mathrm{d}t}\right)\underline{i}^{\mathrm{r}}_{\mathrm{r},p-1}+\frac{\mathrm{d}\underline{\phi}^{\mathrm{r}}_{\mathrm{r},p-1}}{\mathrm{d}t}=0\\
\left(R_{\mathrm{r},p+1}+L_{\acute{\mathrm{o}}\mathrm{r},p+1}\frac{\mathrm{d}}{\mathrm{d}t}\right)\underline{i}^{\mathrm{r}}_{\mathrm{r},p+1}+\frac{\mathrm{d}\underline{\phi}^{\mathrm{r}}_{\mathrm{r},p+1}}{\mathrm{d}t}=0
\end{aligned} \quad (17)$$

where $L_{\acute{o}r,p\pm1}$ are damper winding leakage inductances for the corresponding harmonic, $R_{r,p\pm1}$ are resistances of the damper winding loops for the corresponding harmonic.

As mentioned, the stator connection type, with the neighbouring pole windings connected in series and opposite pole windings in parallel, was considered in this work. The analysis is also suitable for a machine having as many parallel stator windings as there are poles. The flux linkages through the parallel paths of such a winding have the same magnitude, but are phase-shifted with respect to each other. For a magnetic flux harmonic having wave number v, the phase shift between the neighbouring parallel windings is given as

$$\gamma_v = \frac{2\pi v}{N_{pp}} \tag{18}$$

where N_{pp} is the number of parallel paths in the stator winding.

Now, it can be readily verified that $p\pm1$ magnetic flux harmonics through every parallel stator winding are phase-shifted by an angle of $2\pi/N_{pp}$ with respect to each other and their net vector sum gives zero, therefore, assuming the impedances of the parallel windings to be identical, the stator winding can be studied as a symmetric balanced N_{pp}-phase circuit. Thus, the voltage equations for $p\pm1$ harmonics in the stator winding are

$$\begin{aligned}\left(R_{s,p-1} + L_{\acute{o}s,p-1}\frac{d}{dt}\right)\underline{i}^{s}_{s,p-1} + \frac{d\underline{\psi}^{s}_{s,p-1}}{dt} = 0\\ \left(R_{s,p+1} + L_{\acute{o}s,p+1}\frac{d}{dt}\right)\underline{i}^{s}_{s,p+1} + \frac{d\underline{\psi}^{s}_{s,p+1}}{dt} = 0\end{aligned} \tag{19}$$

where $L_{\acute{o}s,p\pm1}$ are parallel stator winding leakage inductances for a corresponding harmonic, $R_{s,p\pm1}$ are parallel stator winding resistances for a corresponding harmonic.

The mains voltage connected to the stator terminals was assumed to consist of the fundamental component only. The path through the stator terminals for nonfundamental current harmonics was considered as a short circuit (the grid, to which the machine was connected, usually has quite small impedance).

By inserting the flux linkage equations into the corresponding voltage equations, the expressions for the current harmonics were obtained. Thus, the currents in the damper winding followed the equations

$$\begin{aligned}&\left(R_{r,p-1} + L_{r,p-1}\frac{d}{dt}\right)\underline{i}^{r}_{r,p-1}\\ &\quad= j\left(s\omega_1 - \omega^{r}_{ecc}\right)\frac{k_{L,r,p-1}}{2\mu_0}\delta_{ecc}B_{p,1}\\ &\qquad\times e^{-j((s\omega_1-\omega^{r}_{ecc})t-\varphi_p+\varphi_{ecc.0})} - k_{cs,p-1}k_{L,r,p-1}\frac{d\underline{i}^{r}_{s,p-1}}{dt}\\ &\left(R_{r,p+1} + L_{r,p+1}\frac{d}{dt}\right)\underline{i}^{r}_{r,p+1}\\ &\quad= j(s\omega_1 + \omega^{r}_{ecc})\frac{k_{L,r,p+1}}{2\mu_0}\delta_{ecc}B_{p,1}\\ &\qquad\times e^{-j((s\omega_1+\omega^{r}_{ecc})t-\varphi_p-\varphi_{ecc.0})} - k_{cs,p+1}k_{L,r,p+1}\frac{d\underline{i}^{r}_{s,p+1}}{dt}\end{aligned} \tag{20}$$

where $L_{s,p\pm1} = L_{\acute{o}r,p\pm1} + L_{self,r,p\pm1}$ are complete inductances of the damper winding for the corresponding magnetic-flux-density waves.

The currents in the parallel stator windings were expressed as

$$\begin{aligned}&\left(R_{s,p-1} + L_{s,p-1}\frac{d}{dt}\right)\underline{i}^{s}_{s,p-1}\\ &\quad= j(\omega_1 - \omega_{ecc})\frac{k_{L,s,p-1}}{2\mu_0}\delta_{ecc}B_{p,1}\\ &\qquad\times e^{-j((\omega_1-\omega_{ecc})t-\varphi_p+\varphi_{ecc.0})} - k_{cr,p-1}k_{L,s,p-1}\frac{d}{dt}\underline{i}^{s}_{r,p-1}\\ &\left(R_{s,p+1} + L_{s,p+1}\frac{d}{dt}\right)\underline{i}^{s}_{s,p+1}\\ &\quad= j(\omega_1 + \omega_{ecc})\frac{k_{L,s,p+1}}{2\mu_0}\delta_{ecc}B_{p,1}\\ &\qquad\times e^{-j((\omega_1+\omega_{ecc})t-\varphi_p-\varphi_{ecc.0})} - k_{cr,p+1}k_{L,s,p+1}\frac{d}{dt}\underline{i}^{s}_{r,p+1}\end{aligned} \tag{21}$$

where $L_{s,p\pm1} = L_{\acute{o}s,p\pm1} + L_{self,s,p\pm1}$ are complete inductances of the parallel stator windings for the corresponding magnetic-flux-density waves.

Note that (20) and (21) show that there exists a coupling between the corresponding current harmonics flowing in the stator and damper windings.

2.6 Solving the current harmonics

To solve the current harmonics flowing in the damper winding, the corresponding current harmonics in the stator winding have to be expressed in the rotor frame of reference and substituted into the expression for the damper winding currents. Whereas, the stator current harmonics can be solved using the rotor current harmonics expressed in the stator reference frame. The co-ordinate system transformation was performed according to these rules

$$\begin{aligned}\underline{i}^{s}_{r,p\pm1} &= \underline{i}^{r}_{r,p\pm1}e^{-j(p\pm1)\Omega_m t}\\ \underline{i}^{r}_{s,p\pm1} &= \underline{i}^{s}_{s,p\pm1}e^{j(p\pm1)\Omega_m t}\\ \frac{d\underline{i}^{s}_{r,p\pm1}}{dt} &= \frac{d\underline{i}^{r}_{r,p\pm1}}{dt}e^{-j(p\pm1)\Omega_m t} - j(p\pm1)\Omega_m\underline{i}^{s}_{r,p\pm1}\\ \frac{d\underline{i}^{r}_{s,p\pm1}}{dt} &= \frac{d\underline{i}^{s}_{s,p\pm1}}{dt}e^{j(p\pm1)\Omega_m t} + j(p\pm1)\Omega_m\underline{i}^{r}_{s,p\pm1}\end{aligned} \tag{22}$$

Using (22) and Laplace transform, the $p-1$ current harmonic in the damper winding was solved. The steady-state solution was

$$\begin{aligned}\underline{i}^{r}_{r,p-1} = \left(s\omega_1 - \omega^{r}_{ecc}\right)&\frac{\left((\omega_1-\omega_{ecc})\left(L_{s,p-1} - k_{cs,p-1}k_{L,s,p-1}\right) + jR_{s,p-1}\right)k_{L,r,p-1}\delta_{ecc}B_{p,1}}{2\mu_0 A_{p-1}\left(\underline{S}_{r,p-1,1} + j\left(s\omega_1 - \omega^{r}_{ecc}\right)\right)\left(\underline{S}_{r,p-1,2} + j\left(s\omega_1 - \omega^{r}_{ecc}\right)\right)}\\ &\times e^{-j\left(\left(s\omega_1-\omega^{r}_{ecc}\right)t-\varphi_p+\varphi_{ecc.0}\right)}\end{aligned} \tag{23}$$

where $\underline{S}_{r,p-1,1}$ and $\underline{S}_{r,p-1,2}$ are the roots of the characteristic equation $A_{p-1}S^2 + \underline{B}_{r,p-1}S + \underline{C}_{r,p-1} = 0$, S denotes the variable in Laplace domain. Coefficients A_{p-1}, $\underline{B}_{r,p-1}$, and

$\underline{C}_{\mathrm{r},p-1}$ are explicitly written as follows

$$\begin{aligned} A_{p-1} &= L_{\mathrm{r},p-1}L_{\mathrm{s},p-1} - k_{\mathrm{cr},p-1}k_{\mathrm{cs},p-1}k_{\mathrm{L,r},p-1}k_{\mathrm{L,s},p-1} \\ \underline{B}_{\mathrm{r},p-1} &= L_{\mathrm{r},p-1}R_{\mathrm{s},p-1} + L_{\mathrm{s},p-1}R_{\mathrm{r},p-1} + \mathrm{j}(p-1)\Omega_{\mathrm{m}} \\ &\quad \times \left(k_{\mathrm{cr},p-1}k_{\mathrm{cs},p-1}k_{\mathrm{L,r},p-1}k_{\mathrm{L,s},p-1} - L_{\mathrm{r},p-1}L_{\mathrm{s},p-1}\right) \\ \underline{C}_{\mathrm{r},p-1} &= R_{\mathrm{r},p-1}R_{\mathrm{s},p-1} - \mathrm{j}(p-1)\Omega_{\mathrm{m}}L_{\mathrm{s},p-1}R_{\mathrm{r},p-1} \end{aligned} \tag{24}$$

In (23) and (24), the complex notation is employed to denote the complex-valued coefficients, note that these are time-invariant.

The $p-1$ current harmonic in the stator winding was

$$\begin{aligned} \underline{i}^{\mathrm{s}}_{\mathrm{s},p-1} = (\omega_1 - \omega_{\mathrm{ecc}}) &\frac{\left((s\omega_1 - \omega^{\mathrm{r}}_{\mathrm{ecc}})(L_{\mathrm{r},p-1} - k_{\mathrm{cr},p-1}k_{\mathrm{L,r},p-1}) + \mathrm{j}R_{\mathrm{r},p-1}\right)k_{\mathrm{L,s},p-1}\delta_{\mathrm{ecc}}B_{p,1}}{2\mu_0 A_{p-1}\left(\underline{S}_{\mathrm{s},p-1,1} + \mathrm{j}(\omega_1 - \omega_{\mathrm{ecc}})\right)\left(\underline{S}_{\mathrm{s},p-1,2} + \mathrm{j}(\omega_1 - \omega_{\mathrm{ecc}})\right)} \\ &\times \mathrm{e}^{-\mathrm{j}((\omega_1-\omega_{\mathrm{ecc}})t-\varphi_p+\varphi_{\mathrm{ecc.0}})} \end{aligned} \tag{25}$$

where $\underline{S}_{\mathrm{s},p-1,1}$ and $\underline{S}_{\mathrm{s},p-1,2}$ were obtained from the equation $A_{p-1}S^2 + \underline{B}_{\mathrm{s},p-1}S + \underline{C}_{\mathrm{s},p-1} = 0$, with coefficients

$$\begin{aligned} \underline{B}_{\mathrm{s},p-1} &= L_{\mathrm{r},p-1}R_{\mathrm{s},p-1} + L_{\mathrm{s},p-1}R_{\mathrm{r},p-1} + \mathrm{j}(p-1)\Omega_{\mathrm{m}} \\ &\quad \times \left(L_{\mathrm{r},p-1}L_{\mathrm{s},p-1} - k_{\mathrm{cr},p-1}k_{\mathrm{cs},p-1}k_{\mathrm{L,r},p-1}k_{\mathrm{L,s},p-1}\right) \\ \underline{C}_{\mathrm{s},p-1} &= R_{\mathrm{r},p-1}R_{\mathrm{s},p-1} + \mathrm{j}(p-1)\Omega_{\mathrm{m}}L_{\mathrm{r},p-1}R_{\mathrm{s},p-1} \end{aligned} \tag{26}$$

whereas coefficient A_{p-1} was the same as in (24).

The $p+1$ current harmonics were

$$\begin{aligned} \underline{i}^{\mathrm{r}}_{\mathrm{r},p+1} = (s\omega_1 + \omega^{\mathrm{r}}_{\mathrm{ecc}}) &\frac{\left((\omega_1 + \omega_{\mathrm{ecc}})\left(L_{\mathrm{s},p+1} - k_{\mathrm{cs},p+1}k_{\mathrm{L,s},p+1}\right) + \mathrm{j}R_{\mathrm{s},p+1}\right)k_{\mathrm{L,r},p+1}\delta_{\mathrm{ecc}}B_{p,1}}{2\mu_0 A_{p+1}\left(\underline{S}_{\mathrm{r},p+1,1} + \mathrm{j}(s\omega_1 + \omega^{\mathrm{r}}_{\mathrm{ecc}})\right)\left(\underline{S}_{\mathrm{r},p+1,2} + \mathrm{j}(s\omega_1 + \omega^{\mathrm{r}}_{\mathrm{ecc}})\right)} \\ &\times \mathrm{e}^{-\mathrm{j}((s\omega_1+\omega^{\mathrm{r}}_{\mathrm{ecc}})t-\varphi_p-\varphi_{\mathrm{ecc.0}})} \\ \underline{i}^{\mathrm{s}}_{\mathrm{s},p+1} = (\omega_1 + \omega_{\mathrm{ecc}}) &\frac{\left((s\omega_1 + \omega^{\mathrm{r}}_{\mathrm{ecc}})\left(L_{\mathrm{r},p+1} - k_{\mathrm{cr},p+1}k_{\mathrm{L,r},p+1}\right) + \mathrm{j}R_{\mathrm{r},p+1}\right)k_{\mathrm{L,s},p+1}\delta_{\mathrm{ecc}}B_{p,1}}{2\mu_0 A_{p+1}\left(\underline{S}_{\mathrm{s},p+1,1} + \mathrm{j}(\omega_1 + \omega_{\mathrm{ecc}})\right)\left(\underline{S}_{\mathrm{s},p+1,2} + \mathrm{j}(\omega_1 + \omega_{\mathrm{ecc}})\right)} \\ &\times \mathrm{e}^{-\mathrm{j}((\omega_1+\omega_{\mathrm{ecc}})t-\varphi_p-\varphi_{\mathrm{ecc.0}})} \end{aligned} \tag{27}$$

where $\underline{S}_{\mathrm{r},p+1,1}$, $\underline{S}_{\mathrm{r},p+1,2}$, $\underline{S}_{\mathrm{s},p+1,1}$ and $\underline{S}_{\mathrm{s},p+1,2}$ can be obtained by solving the equations $A_{p+1}S^2 + \underline{B}_{\mathrm{r},p+1}S + \underline{C}_{\mathrm{r},p+1} = 0$ and $A_{p+1}S^2 + \underline{B}_{\mathrm{s},p+1}S + \underline{C}_{\mathrm{s},p+1} = 0$, respectively, where the coefficients are given in (24) and (26) with $(p-1)$ replaced by $(p+1)$ in every occasion (indices and multipliers). Note that (27) only contains the steady-state current components.

2.7 Electromagnetic force on the rotor

To calculate the electromagnetic force acting on the rotor, the expression for the radial component of the Maxwell stress tensor was used

$$\sigma(\varphi, t) = \frac{1}{2\mu_0}[B(\varphi, t)]^2 = \frac{1}{2\mu_0}\left[\sum_{v=0}^{\infty}\mathrm{Re}\{\underline{B}_v(\varphi)\mathrm{e}^{\mathrm{j}v\varphi}\}\right]^2 \tag{28}$$

The total electromagnetic force was obtained by integrating the Maxwell stress over the whole circumference of a machine

$$\underline{F}_{\mathrm{e}} = \frac{d_{\mathrm{R}}l_{\mathrm{e}}}{2}\int_0^{2\pi}\sigma(\varphi, t)\cdot\mathrm{e}^{\mathrm{j}\varphi}\,\mathrm{d}\varphi \tag{29}$$

where d_{R} is the outer diameter of the rotor.

The force on the rotor was assumed to be generated by interaction of two magnetic flux density harmonics:

$$\underline{F}_{\mathrm{e}} = \frac{d_{\mathrm{R}}l_{\mathrm{e}}}{8\mu_0}\int_0^{2\pi}\left(\underline{B}_v\underline{B}^*_w\mathrm{e}^{\mathrm{j}(v-w+1)\varphi} + \underline{B}^*_v\underline{B}_w\mathrm{e}^{-\mathrm{j}(v-w-1)\varphi}\right)\mathrm{d}\varphi \tag{30}$$

where symbol '$*$' designates a complex conjugate.

From (30) it is seen that the net force can only be produced by the magnetic-flux-density components with wave numbers satisfying the condition $v - w = \pm 1$. The rotor eccentricity mainly causes the magnetic flux waves with wave numbers $p \pm 1$ (see (11b)). These, together with the fundamental field, satisfy the aforementioned condition for the net force generation, therefore the electromagnetic force due to the rotor eccentricity can be expressed as

$$\begin{aligned} \underline{F}^{\mathrm{s}}_{\mathrm{e}} = \frac{\pi d_{\mathrm{R}}l_{\mathrm{e}}}{4\delta_0}&\left(\frac{B_{p,1}}{\mu_0}\left(B_{p,1} + B_{p,2}\cos\left(2\varphi_p\right)\right)\right. \\ &\times \delta_{\mathrm{ecc}}\mathrm{e}^{\mathrm{j}(\omega_{\mathrm{ecc}}t-\varphi_{\mathrm{ecc.0}})} + \left(B_{p,1}\mathrm{e}^{-\mathrm{j}\varphi_p} + B_{p,2}\mathrm{e}^{\mathrm{j}\varphi_p}\right) \\ &\times \left(k_{\mathrm{cr},p-1}\underline{i}^{\mathrm{s}}_{\mathrm{r},p-1} + k_{\mathrm{cs},p-1}\underline{i}^{\mathrm{s}}_{\mathrm{s},p-1}\right) \\ &\times \mathrm{e}^{\mathrm{j}\omega_1 t} + \left(B_{p,1}\mathrm{e}^{\mathrm{j}\varphi_p} + B_{p,2}\mathrm{e}^{-\mathrm{j}\varphi_p}\right) \\ &\left.\times \left(k_{\mathrm{cr},p+1}\underline{i}^{\mathrm{s}*}_{\mathrm{r},p+1} + k_{\mathrm{cs},p+1}\underline{i}^{\mathrm{s}*}_{\mathrm{s},p+1}\right)\mathrm{e}^{-\mathrm{j}\omega_1 t}\right) \end{aligned} \tag{31}$$

Substituting the current harmonics from (23), (25) and (27) into (31) yielded the expression of the electromagnetic force. Note that in (31) the stator reference frame is used throughout, therefore the rotor current harmonics have to be transformed to this reference frame before being substituted into (31). This can be done using (22), thus the

electromagnetic force can be represented as

$$\underline{F}_{\mathrm{e}}^{\mathrm{s}} = \frac{\pi d_{\mathrm{R}} l_{\mathrm{e}}}{4\mu_0\,\delta_0} B_{p,1} \times \left[\left(B_{p,1} + B_{p,2}\cos(2\varphi_p) \right) + \frac{B_{p,1} + B_{p,2}\mathrm{e}^{\mathrm{j}2\varphi_p}}{2A_{p-1}} \times \left(\begin{array}{c} ((\omega_1 - \omega_{\mathrm{ecc}}) \\ (L_{\mathrm{s},p-1} - k_{\mathrm{cs},p-1}k_{\mathrm{L,s},p-1}) \\ +\mathrm{j}R_{\mathrm{s},p-1})k_{\mathrm{cr},p-1}k_{\mathrm{L,r},p-1} \\ (s\omega_1 - \omega_{\mathrm{ecc}}^{\mathrm{r}}) \dfrac{\left(\underline{S}_{\mathrm{r},p-1,1} + \mathrm{j}(s\omega_1 - \omega_{\mathrm{ecc}}^{\mathrm{r}})\right)}{\times\left(\underline{S}_{\mathrm{r},p-1,2} + \mathrm{j}(s\omega_1 - \omega_{\mathrm{ecc}}^{\mathrm{r}})\right)} \end{array} \right. \right.$$

$$\left. \left. + (\omega_1 - \omega_{\mathrm{ecc}}) \frac{\begin{array}{c} ((s\omega_1 - \omega_{\mathrm{ecc}}^{\mathrm{r}}) \\ (L_{\mathrm{r},p-1} - k_{\mathrm{cr},p-1}k_{\mathrm{L,r},p-1}) \\ +\mathrm{j}R_{\mathrm{r},p-1})k_{\mathrm{cs},p-1}k_{\mathrm{L,s},p-1} \end{array}}{\begin{array}{c} \left(\underline{S}_{\mathrm{s},p-1,1} + \mathrm{j}(\omega_1 - \omega_{\mathrm{ecc}})\right) \\ \times\left(\underline{S}_{\mathrm{s},p-1,2} + \mathrm{j}(\omega_1 - \omega_{\mathrm{ecc}})\right) \end{array}} \right) + \frac{B_{p,1} + B_{p,2}\mathrm{e}^{-\mathrm{j}2\varphi_p}}{2A_{p+1}} \times \left(\begin{array}{c} ((\omega_1 + \omega_{\mathrm{ecc}}) \\ (L_{\mathrm{s},p+1} - k_{\mathrm{cs},p+1}k_{\mathrm{L,s},p+1}) \\ -\mathrm{j}R_{\mathrm{s},p+1})k_{\mathrm{cr},p+1}k_{\mathrm{L,r},p+1} \\ (s\omega_1 + \omega_{\mathrm{ecc}}^{\mathrm{r}}) \dfrac{\left(\underline{S}^*_{\mathrm{r},p+1,1} - \mathrm{j}(s\omega_1 + \omega_{\mathrm{ecc}}^{\mathrm{r}})\right)}{\times\left(\underline{S}^*_{\mathrm{r},p+1,2} - \mathrm{j}(s\omega_1 + \omega_{\mathrm{ecc}}^{\mathrm{r}})\right)} \end{array} \right.$$

$$\left. \left. + (\omega_1 + \omega_{\mathrm{ecc}}) \frac{\begin{array}{c} ((s\omega_1 + \omega_{\mathrm{ecc}}^{\mathrm{r}}) \\ (L_{\mathrm{r},p+1} - k_{\mathrm{cr},p+1}k_{\mathrm{L,r},p+1}) \\ -\mathrm{j}R_{\mathrm{r},p+1})k_{\mathrm{cs},p+1}k_{\mathrm{L,s},p+1} \end{array}}{\begin{array}{c} \left(\underline{S}^*_{\mathrm{s},p+1,1} - \mathrm{j}(\omega_1 + \omega_{\mathrm{ecc}})\right) \\ \times\left(\underline{S}^*_{\mathrm{s},p+1,2} - \mathrm{j}(\omega_1 + \omega_{\mathrm{ecc}})\right) \end{array}} \right) \right] \delta_{\mathrm{ecc}}\mathrm{e}^{\mathrm{j}(\omega_{\mathrm{ecc}}t - \varphi_{\mathrm{ecc},0})} \quad (32)$$

Equation (32) is a parametric model representing the electromagnetic force on the whirling rotor, as a function of whirling radius and whirling angular speed. The model has twenty real-valued physical parameters (the term $\partial d_{\mathrm{R}} l_{\mathrm{e}}/4\mu_0\delta_0$ was regarded as an unknown parameter), which can be estimated from numerical simulation results. Thus, the model accounts for the effects of iron core saturation, slotting and equalising currents in the damper winding and parallel stator windings, because all these phenomena were considered in the simulation. The force model can also be represented as

$$\underline{K}(\mathrm{j}\omega_{\mathrm{ecc}}) = \frac{\underline{F}_{\mathrm{e}}^{\mathrm{s}}}{\delta_{\mathrm{ecc}}\mathrm{e}^{\mathrm{j}(\omega_{\mathrm{ecc}}t - \varphi_{\mathrm{ecc},0})}} = \frac{\pi d_{\mathrm{R}} l_{\mathrm{e}}}{4\mu_0\,\delta_0} B_{p,1} \left[\left(B_{p,1} + B_{p,2}\cos(2\varphi_p) \right) + \frac{B_{p,1} + B_{p,2}\mathrm{e}^{\mathrm{j}2\varphi_p}}{2A_{p-1}} \times \left(\begin{array}{c} ((\omega_1 - \omega_{\mathrm{ecc}}) \\ (L_{\mathrm{s},p-1} - k_{\mathrm{cs},p-1}k_{\mathrm{L,s},p-1}) \\ +\mathrm{j}R_{\mathrm{s},p-1})k_{\mathrm{cr},p-1}k_{\mathrm{L,r},p-1} \\ (s\omega_1 - \omega_{\mathrm{ecc}}^{\mathrm{r}}) \dfrac{\left(\underline{S}_{\mathrm{r},p-1,1} + \mathrm{j}(s\omega_1 - \omega_{\mathrm{ecc}}^{\mathrm{r}})\right)}{\times\left(\underline{S}_{\mathrm{r},p-1,2} + \mathrm{j}(s\omega_1 - \omega_{\mathrm{ecc}}^{\mathrm{r}})\right)} \end{array} \right. \right.$$

$$\left. \left. + (\omega_1 - \omega_{\mathrm{ecc}}) \frac{\begin{array}{c} ((s\omega_1 - \omega_{\mathrm{ecc}}^{\mathrm{r}}) \\ (L_{\mathrm{r},p-1} - k_{\mathrm{cr},p-1}k_{\mathrm{L,r},p-1}) \\ +\mathrm{j}R_{\mathrm{r},p-1})k_{\mathrm{cs},p-1}k_{\mathrm{L,s},p-1} \end{array}}{\begin{array}{c} \left(\underline{S}_{\mathrm{s},p-1,1} + \mathrm{j}(\omega_1 - \omega_{\mathrm{ecc}})\right) \\ \times\left(\underline{S}_{\mathrm{s},p-1,2} + \mathrm{j}(\omega_1 - \omega_{\mathrm{ecc}})\right) \end{array}} \right) + \frac{B_{p,1} + B_{p,2}\mathrm{e}^{-\mathrm{j}2\varphi_p}}{2A_{p+1}} \times \left(\begin{array}{c} ((\omega_1 + \omega_{\mathrm{ecc}}) \\ (L_{\mathrm{s},p+1} - k_{\mathrm{cs},p+1}k_{\mathrm{L,s},p+1}) \\ -\mathrm{j}R_{\mathrm{s},p+1})k_{\mathrm{cr},p+1}k_{\mathrm{L,r},p+1} \\ (s\omega_1 + \omega_{\mathrm{ecc}}^{\mathrm{r}}) \dfrac{\left(\underline{S}^*_{\mathrm{r},p+1,1} - \mathrm{j}(s\omega_1 + \omega_{\mathrm{ecc}}^{\mathrm{r}})\right)}{\times\left(\underline{S}^*_{\mathrm{r},p+1,2} - \mathrm{j}(s\omega_1 + \omega_{\mathrm{ecc}}^{\mathrm{r}})\right)} \end{array} \right.$$

$$\left. \left. + (\omega_1 + \omega_{\mathrm{ecc}}) \frac{\begin{array}{c} ((s\omega_1 + \omega_{\mathrm{ecc}}^{\mathrm{r}}) \\ (L_{\mathrm{r},p+1} - k_{\mathrm{cr},p+1}k_{\mathrm{L,r},p+1}) \\ -\mathrm{j}R_{\mathrm{r},p+1})k_{\mathrm{cs},p+1}k_{\mathrm{L,s},p+1} \end{array}}{\begin{array}{c} \left(\underline{S}^*_{\mathrm{s},p+1,1} - \mathrm{j}(\omega_1 + \omega_{\mathrm{ecc}})\right) \\ \times\left(\underline{S}^*_{\mathrm{s},p+1,2} - \mathrm{j}(\omega_1 + \omega_{\mathrm{ecc}})\right) \end{array}} \right) \right] \quad (33)$$

where $\underline{K}(\mathrm{j}\omega_{\mathrm{ecc}})$ is a frequency response function (FRF) of the electromagnetic force. Note that $\underline{K}(\mathrm{j}\omega_{\mathrm{ecc}})$ is independent of time and the complex notation only signifies that it is complex-valued.

2.8 Numerical calculation

The numerical calculation of the magnetic field was based on the transient time-stepping finite-element analysis (FEA) [14]. The magnetic field and circuit equations were discretised and solved together as a system of equations. The time-dependence of the variables was modelled by Crank-Nicholson method. The forces were calculated at each time-step using a method developed by Coulomb [15].

Several simplifications were made to keep the amount of computation at a reasonable level. The magnetic field in the core region was assumed to be two-dimensional. The laminated iron core was treated as a nonconducting magnetically nonlinear medium, and the nonlinearity was modelled by a single-valued magnetisation curve. Modelling of the air gap regions also was two-dimensional. The rotor motion was facilitated by changing the shapes of the finite elements (FE) in the air gap.

The impulse method [16] was implemented in the FEA, which allowed the FRF of the force, in the whole studied whirling frequency range ([−100, 100] Hz), to be obtained using the results of a single numerical simulation, thus significantly reducing the computation time.

All numerical calculations were carried out on a PC powered by AMD Athlon 64 3000+ processor. The synchronous machine was simulated using first-order FE. The FE model contained 7344 nodes. Two seconds of the machine performance required three hours of computation time. The induction machine was simulated using second-order FE; its model contained 16 953 nodes. To simulate one second of the machine operation required approximately five hours of computation time.

3 Results

To estimate the force model parameters, the aforementioned salient-pole synchronous machine was simulated using the FEA. The main parameters of the machine are listed in Table 2.

The machine was operated in a steady-state generator mode and connected to a balanced line voltage. The mechanical angular velocity of the rotor was kept constant. The machine had four parallel stator windings and the damper winding.

The FRF of the force obtained from the numerical simulation is shown in Fig. 3. This complex-valued FRF was resolved into real and imaginary parts, which correspond to radial (continuous curve) and tangential (dashed curve) force components, respectively. The radial force component acts in the direction of the shortest air gap and the tangential one is directed orthogonally to it. The radial and tangential force components rotate together with the point of the shortest air gap. The tangential component of the electromagnetic force due to the rotor eccentricity must be distinguished from the tangential force responsible for the machine's torque generation during the normal operation.

The force model parameters were calculated from these results employing a genetic-algorithms-based estimation program. The estimated force model parameters are listed

Table 2: Main parameters of simulated synchronous machine

Parameter	Value
Number of pole-pairs	4
Number of parallel stator windings	4
Frequency of the voltage supplied to the stator winding, Hz	50
Stator winding supply voltage, V	6300
Field winding supply voltage, V	150
Stator winding connection	Star
Apparent power, kVA	8400
Power factor	0.83 Cap.

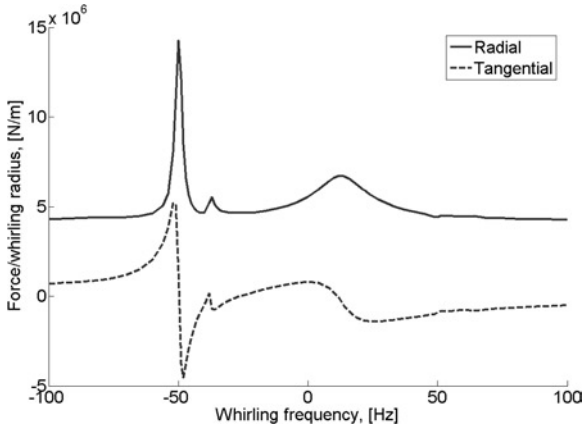

Fig. 3 *FRF of electromagnetic force obtained from a numerical simulation*

in Table 3 which also contains the estimated parameters for the other test motor.

To evaluate the performance of the presented force model, these parameters were substituted into the force model expression (33). By doing this, the estimated FRF of the force was obtained. Comparison of the estimated FRF and the original FRF from the FEA is shown in Fig. 4.

The performance of the parametric force model, when applied to an induction machine, was also studied. Table 4 lists the main parameters of the second test-motor, which had six parallel stator windings and the rotor cage. In this machine, the fundamental field was generated by the stator winding and rotor cage, and the rotor surface was cylindrical (no saliency), therefore the magnetic flux density term $B_{p,2}$ (in (33)) was equal to zero and the force model expression became slightly simpler. By forcing $B_{p,2} = 0$, the term $(\pi d_R l_e/4\mu_0\delta_0)B_{p,1}^2$ can be estimated as a single parameter, thus reducing the number of unknown

Table 3: Estimated force model parameters

Parameter	Synchronous machine Value	Induction machine Value
$\pi d_r l_e/4\mu_0\delta_0$	5.18×10^{6}	—
$L_{r,p+1}$	8.99×10^{-2}	-9.70×10^{-3}
$L_{s,p+1}$	1.72×10^{-2}	2.70×10^{-2}
$L_{r,p-1}$	6.52×10^{-2}	-2.25×10^{-2}
$L_{s,p-1}$	-3.89×10^{-2}	1.23×10^{-2}
$R_{r,p+1}$	4.37×10^{2}	6.53×10^{1}
$R_{s,p+1}$	1.72×10^{-1}	2.49
$R_{r,p-1}$	5.78	−2.04
$R_{s,p-1}$	-3.58×10^{-1}	1.44
$k_{cr,p+1}$	3.32×10^{-1}	-2.14×10^{-2}
$k_{cs,p+1}$	5.72	−4.31
$k_{cr,p-1}$	1.30	3.52×10^{-1}
$k_{cs,p-1}$	3.38×10^{-1}	-3.95×10^{-2}
$k_{L,r,p+1}$	2.57×10^{-2}	1.12×10^{-1}
$k_{L,s,p+1}$	3.65×10^{-3}	-3.14×10^{-3}
$k_{L,r,p-1}$	1.42×10^{-2}	-4.71×10^{-3}
$k_{L,s,p-1}$	3.52×10^{-3}	-2.95×10^{-2}
$B_{p,1}$	1.74	—
$B_{p,2}$	9.93×10^{-2}	—
φ_p	-3.51×10^{-1}	—
$(\pi d_r l_e/4\mu_0\delta_0)B_{p,1}^2$	—	2.26×10^{6}

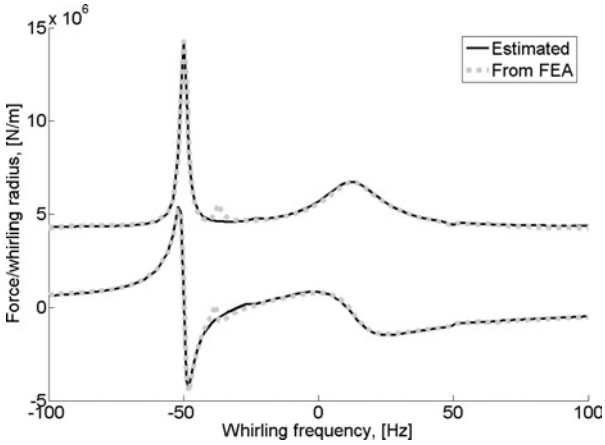

Fig. 4 *Comparing estimated FRF against FRF from numerical simulation for synchronous machine*

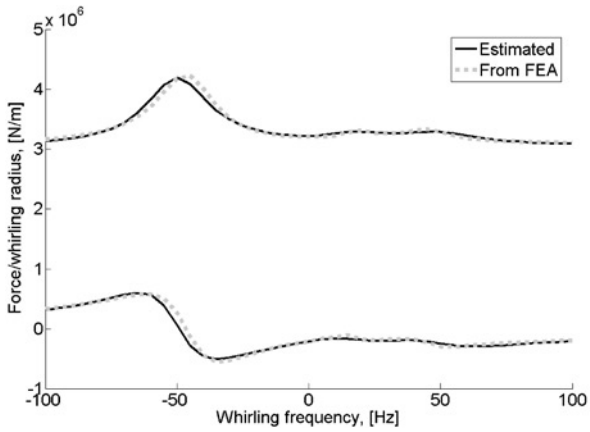

Fig. 5 *Comparing estimated FRF against FRF from numerical simulation for induction machine*

parameters to seventeen. Table 3 lists the estimated force model parameters for this machine. Fig. 5 demonstrates the performance of the force model with the estimated parameters.

4 Discussion

UMP analysis in electrical machines, equipped with both the parallel stator windings and damper winding (rotor cage), becomes especially complicated, as the effects of the equalising currents flowing in the stator and rotor have to be accounted for. Moreover, the coupling between the stator and rotor equalising currents also needs to be considered.

As the frequency of the electromagnetic force associated with rotor eccentricity is often lower than that of the fundamental field [16], the whirling frequency range of interest was chosen to be $[-100, 100]$ Hz.

As the rotor eccentricity engenders mainly the magnetic fields having wave numbers $p \pm 1$, only these interacting with the fundamental field were considered in the analytical part and included in the force model. The effects of the remaining magnetic field harmonics, e.g. slot harmonics, were approximately taken into account by the term $(\pi d_r l_e/4\mu_0\delta_0)B_{p,1}$ (see (33)), which is independent of the whirling frequency.

According to (25) and (27), the $p \pm 1$ stator current harmonics vanish as the whirling frequency approaches ∓ 50 Hz, respectively. Hence, at these particular whirling frequency values, the parallel stator windings do not damp the corresponding magnetic-flux-density harmonics and only the damper winding affects their magnitude.

Table 4: Main parameters of induction machine

Parameter	Value
Number of pole-pairs	3
Rated frequency, Hz	50
Rated voltage, V	400
Rated power, kW	18.5
Rated slip	0.0145
Connection type	Delta
Skew of the rotor slots	0
Number of parallel stator windings	6

At -50 Hz, where the $p+1$ stator current harmonic is zero, the radial force component has the maximum value (see Fig. 3). Thus, it can be concluded that the $p+1$ magnetic field harmonic plays a more important role in the UMP generation than the $p-1$ harmonic. As for the $p-1$ magnetic field harmonic, although at 50 Hz the stator winding does not affect it, the damper winding seems to have a very strong influence on this magnetic field wave. Therefore, the radial UMP component does not peak at this whirling frequency value.

According to (23) and (27), the $p \pm 1$ eccentricity fields become stationary with respect to the damper winding when, respectively

$$\omega_{ecc} = \omega_1\left(\frac{1}{p} - s\left(\frac{1}{p} \pm 1\right)\right)$$

For synchronous machines (and for induction machines at no-load), this condition is simply $\omega_{ecc} = \omega_1/p$, therefore, in Fig. 3 at 12.5 Hz (8-pole synchronous machine, 50 Hz supply frequency) the radial force component peaks.

In the case of a synchronous machine, there was observed a small sharp peak in the radial force component at -37.5 Hz (see Fig. 3). The phenomenon behind this peak is not clear yet, but we suppose that it could be due to the coupling between eccentricity fields with other magnetic field harmonics, which are produced by the currents in the parallel stator windings.

Fig. 4 shows that the FRF of the force, obtained by substituting the estimated parameters into the force model expression (33), agrees very well with the FRF calculated by the FEA. This excellent model performance is exhibited throughout the whole studied whirling frequency range. The peak at -37.5 Hz is not described by the estimated FRF as its origins were not considered in the force model presented.

Inspecting (33) it is seen that the only term pertinent to the rotor saliency is the constituent of the fundamental magnetic flux density $B_{p,2}$. Thus, eliminating the influence of the rotor saliency would only have a minor influence on the parametric force model, therefore the model was also applied to an induction machine, having parallel stator windings and the rotor cage. It is worth noting that, in a loaded induction machine, the fundamental field is also being produced by the corresponding current in the rotor cage. If this current was included into the analysis, it would become a constituent of $B_{p,1}$ in (14) and have no effect on the remaining equations.

When studying the induction machine (Fig. 5), interesting phenomena were observed:

1. Peaks in the radial FRF component due to the eccentricity fields $p \pm 1$ being stationary with respect to the stator are not anymore located at ∓ 50 Hz.
2. Peaks in the radial FRF component due to the eccentricity fields $p \pm 1$ being stationary with respect to the rotor do not occur at the whirling angular speeds:

$$\omega_{ecc} = \omega_1 \left(\frac{1}{p} - s\left(\frac{1}{p} \pm 1 \right) \right)$$

The authors believe that these phenomena are due to the interactions occurring between the currents induced by the eccentricity fields in the parallel stator windings and the currents induced by the same fields in the rotor cage. In induction machines, these interactions could be stronger than they are in synchronous machines due to the smaller air gap (that provides larger mutual inductances between the stator and rotor windings) and different structure of the rotor cage.

As seen in Fig. 5, the performance of the developed force model is also very good when applied to an induction machine. The force model developed has also been applied to the same synchronous and induction machines that were now equipped with either the parallel stator windings or the rotor cage. In all those tests, the model also performed very well, however these results are not presented in this paper.

It is also worth mentioning that the estimated set of force model parameters corresponds to a certain operating point (supply voltage, load torque etc.) of a machine. Slot harmonics are considered as one of the main reasons for the electromagnetic force dependence on the loading. These have a very small whirling frequency dependence in the range considered, but can vary significantly due to the load changes. Moreover, the configuration of the stator winding may have a profound effect on the shape of FRF of the force, therefore different sets of parameters may have to be used for the same machine with different stator winding connections.

5 Conclusions

A low-order parametric force model, for the electromagnetic force in eccentric rotor electrical machines equipped with both the parallel stator windings and damper winding (rotor cage), was developed and verified in this paper using two example motors. The model was based on permeance harmonic analysis and included the effects of equalising currents flowing in the stator and rotor windings separately, and also the effects of the interaction between these currents. Moreover, the model accounted also for the effects of iron core saturation and stator and rotor slotting. In the whole whirling frequency range studied, results from the force model agreed very well with the results from numerical calculations, when applied to synchronous machines as well as to induction machines.

The proposed force model has the following advantages:

1. It allows simple, quick and accurate calculation of the electromagnetic force at a desired whirling frequency value or in a certain range of whirling frequencies;
2. The same model parameters can be directly used at different values of whirling radius (as the force has a linear dependence on the rotor displacement [17]) and whirling frequency;
3. The model offers an attractive opportunity to be integrated into the mechanical analysis to study electromechanical interactions in electrical machines;
4. The model can be successfully used with synchronous machines and induction machines. Moreover, the model proved to be very accurate when applied to electrical machines equipped with either the parallel stator windings or the rotor cage.

If the operating point (supply voltage, load torque etc.) of a machine is changed, or if the stator winding configuration is modified, the force model parameters have to be re-estimated.

6 References

1 Fisher-Hinnen, J.: 'Dynamo design' (Van Nostrand, 1899)
2 Hellmund, R.E.: 'Series versus parallel windings for a.c. motors', *Electr. World*, 1907, **49**, pp. 388–389
3 Krondl, M.: 'Self excited radial vibrations of the rotor of induction machines with parallel paths in the winding', *Bull. Assoc. Suisse, Electr.*, 1956, **47**, pp. 581–588
4 Ellison, A.J., and Yang, S.J.: 'Effects of rotor eccentricity on acoustic noise from induction machines', *Proc. Inst. Electr. Eng.*, 1977, **118**, (1), pp. 174–183
5 Arkkio, A., and Lindgren, O.: 'Unbalanced magnetic pull in a high-speed induction motor with an eccentric rotor'. Proc. Int. Conf. Electr. Mach., Paris, France, 5–8 September 1994, vol. 1, pp. 53–58
6 Dorrell, D.G., and Smith, A.C.: 'Calculation of UMP in induction motors with series or parallel winding connections', *IEEE Trans. Energy Convers.*, 1994, **9**, (2), pp. 304–310
7 DeBortoli, M.J., Salon, S.J., Burow, D.W., and Slavik, C.J.: 'Effects of rotor eccentricity and parallel windings on induction machine behaviour: a study using finite element analysis', *IEEE Trans. Magn.*, 1993, **29**, (2), pp. 1676–1682
8 Früchtenicht, J., Jordan, H., and Seinsch, H.O.: 'Exzentrizitätsfelder als Ursache von Lafinstabilitäten bei Asynchronmaschinen. Teil I und II', *Arch. Elektrotech.*, 1982, **65**, pp. 271–292
9 Arkkio, A., Antila, M., Pokki, K., Simon, A., and Lantto, E.: 'Electromagnetic force on a whirling cage rotor', *IEE Proc., Electr. Power Appl.*, 2000, **147**, pp. 353–360
10 Burakov, A., and Arkkio, A.: 'Low-order parametric force model for a salient-pole synchronous machine with eccentric rotor', *Electr. Eng. (Arch. Elektrotech.)*, 2006, **89**, (2), pp. 127–136
11 Burakov, A., and Arkkio, A.: 'Low-order parametric force model for eccentric-rotor electrical machine with parallel connections in the stator winding', *IEE Proc., Electr. Power Appl.*, **153**, (4), pp. 592–600
12 Shi, C., and Li, M.: 'A general model of synchronous machine for its steady-state performance analysis', *IEEE Trans. Energy Convers.*, 1990, **5**, (3), pp. 531–537
13 Richter, R.: 'Elektrische Maschinen Zweiter Band' (Verlag Birkhäuser, Basel/Stuttgart, 1953), p. 707
14 Arkkio, A.: 'Analysis of induction motors based on the numerical solution of the magnetic field and circuit equations', *Acta Polytech. Scand., Electr. Eng. Ser.*, 1987, (59), Helsinki, 97 pp.
15 Coulomb, J.L.: 'A methodology for the determination of global electromechanical quantities from a finite element analysis and its application to the evaluation of magnetic forces, torques and stiffness', *IEEE Trans. Magn.*, 1983, **19**, (6), pp. 2514–2519
16 Tenhunen, A., Holopainen, T.P., and Arkkio, A.: 'Impulse method to calculate the frequency response of the electromagnetic forces on whirling cage rotors', *IEE Proc., Electr. Power Appl.*, 2003, **150**, (6), pp. 752–756
17 Tenhunen, A., Holopainen, T.P., and Arkkio, A.: 'Spatial linearity of unbalanced magnetic pull in induction motors during eccentric rotor motions', *COMPEL: Int. J. Comput. Math. Electr. Electron. Eng.*, 2003, **22**, (4), pp. 862–876